Kovasznay mode–preserving and entropy-stable numerical methods

By A. Cicchino AND P. Moin

Entropy-stable, kinetic energy–stable, and nonlinearly stable numerical methods have gained popularity in computational fluid dynamics because they guarantee robustness on coarse meshes. Although nonlinear stability ensures that perturbations caused by aliasing errors remain bounded, as proven by Nordström (2022), underresolved flow simulations can still suffer—Gassner *et al.* (2022) demonstrated that the bounded perturbations may introduce spurious oscillations that cause nonphysical results, such as negative density. We use the theory from Kovasznay's modal decomposition and Ribner's linear interaction analysis to present a set of weak conservation conditions termed Kovasznay mode preservation (KMP). Here, KMP is added to both entropy and kinetic energy conservation. We demonstrate how to satisfy KMP in skew-symmetric finite-volume and uncollocated discontinuous Galerkin methods. Numerically, for inviscid compressible flows, we demonstrate that KMP provides insight into the propagation of spurious modes downstream of a shock, and we evaluate its impact on shock–vortex and shock–entropic interactions on coarse, underresolved meshes.

1. Introduction

Entropy-stable, kinetic energy–stable, and nonlinearly stable numerical methods guarantee robustness on coarse meshes, making them popular in computational fluid dynamics. Tadmor (1984) proved that if the numerical flux satisfies the entropy condition from Harten (1983), then the discretization is entropy stable. Entropy stability was accomplished by introducing a weak condition on the numerical flux, commonly referred to as the Tadmor shuffle condition. These ideas were extended by LeFloch & Rohde (2000) and LeFloch *et al.* (2002) in the context of high-order finite-difference stencils. Honein & Moin (2004) derived an entropy-conserving (EC) and kinetic energy–preserving (KEP) split form by considering a higher-order entropy function. KEP methods have been demonstrated to successfully decouple the numerical dissipation caused by aliasing errors from subgrid-scale models for large-eddy simulation (LES) of incompressible and compressible flows (Morinishi *et al.* 1998; Moin 2002; Honein & Moin 2004; Mahesh *et al.* 2006; Moin & Apte 2006; Ham *et al.* 2007; Goc *et al.* 2021; Jain & Moin 2022).

Moving toward strongly compressible turbulent flows in the presence of shocks, we anticipate that entropy-stability must be paired with kinetic energy preservation to have similar effects in LES for postshock statistical quantities of interest, such as kinetic energy amplification. In the last decade, the skew-symmetric kinetic energy and entropy-stable framework was expanded to bounded domains by Fisher & Carpenter (2013), who combined summation-by-parts (SBP) methods with Tadmor's two-point flux functions to achieve entropy-conservation. Extending the connection made by Fisher & Carpenter (2013) between the SBP framework and Tadmor's shuffle condition, entropy-conservative and -stable methods have been successfully implemented in discontinuous Galerkin (DG) methods (Gassner 2013; Gassner *et al.* 2016; Chan 2018, 2019; Montoya & Zingg 2024),

residual distribution schemes (Abgrall 2018; Abgrall *et al.* 2021, 2022), and nonlinearly stable flux reconstruction (NSFR) (Cicchino *et al.* 2022a,b; Cicchino & Nadarajah 2025).

Gassner *et al.* (2022) demonstrated that discretely entropy-stable and kinetic energy–stable methods can suffer from a local linear instability. As explained by Nordström (2022), the dual relationship between nonlinear stability and linear stability proves that any perturbation's growth stays bounded. Nordström (2022) then proved that the local energy stability issues raised by Gassner *et al.* (2022) are technically not global linear stability issues. The results obtained by Gassner *et al.* (2022, Figure 11-14) confirm the global linear stability bound because the perturbation grows with the largest positive eigenvalue and then plateaus. The ability of the scheme to experience a local linear instability is a preferred property because positive eigenvalues in the residual's Jacobian have historically been used to predict the transition to turbulence, as used in the eN method (Van Ingen 2008).

The purpose of this research brief is to predict the fictitious forces that may be introduced by dispersive errors present in the numerical discretization. To accomplish this goal, we conjecture that aliasing errors present in the numerical discretization are dominated by the transport of the linear perturbation—much like the physical process of shock–turbulence interaction. Ribner (1954) used Kovasznay's (1953) modal decomposition to derive linear interaction analysis (LIA), a model for predicting postshock kinetic energy amplification for shock–turbulence interaction. LIA assumes that when isotropic turbulent flow interacts with a shock, the immediate postshock forces are dominated by the linear modes. Thus, LIA decomposes the isotropic turbulence into the entropic, vortical, and acoustic modes and considers each mode's interaction with the shock independently. Lee *et al.* (1993, 1997) were the first to numerically verify LIA for shock–turbulence interaction by considering the amplification caused by the vortical mode interacting with the shock. Then, Mahesh *et al.* (1995, 1997) extended this analysis to incorporate acoustic modes and entropic-vortical modes, finding that a negative correlation between velocity and temperature leads to an enhanced turbulence amplification postshock, and vice versa. Building on the work by Lee *et al.* (1993, 1997), Larsson & Lele (2009) performed direct numerical simulations of canonical shock–turbulence interaction. Through Kolmogorov scaling arguments, they showed that grid refinement is needed to resolve all scales of the shock corrugations in both the shock normal and transverse directions. Bermejo & Lele (2010) then considered LES of shock–turbulence interaction and found that the shock corrugations need to be fully resolved with subgrid-scale models that are active only downstream of the shock because of the dissipative nature of weighted essentially nonoscillatory schemes (Johnsen *et al.* 2010).

In Section 2, we introduce the compressible Euler equations and the concepts of entropy/kinetic energy stability. In Section 2.1, we briefly present the NSFR method (Cicchino & Nadarajah 2025) that we use for numerical tests. In Section 3, we present the KMP conditions and prove their impact on the discretization of the pressure in the momentum equations. Lastly, in Section 4, we numerically investigate an underresolved shock–vortex interaction and a one-dimensional shock–entropy interaction to investigate the effect of KMP on the Kovasznay modes downstream of the shock.

2. Mathematical background

First, we introduce the background of entropy stability for a general conservation law, then apply it to the compressible Euler equations.

Consider the system of 3D conservation laws,

$$\begin{gathered}\frac{\partial}{\partial t}u_i\left(\boldsymbol{x}^c,t\right)+\nabla\cdot\boldsymbol{f}_i\left(\boldsymbol{u}\left(\boldsymbol{x}^c,t\right)\right)=0,\ \forall i\in[1,n_{\text{state}}],\ t\geq 0,\ \boldsymbol{x}^c\coloneqq[x\ y\ z]\in\Omega,\\ u_i(\boldsymbol{x}^c,0)=u_{i,0}\left(\boldsymbol{x}^c\right),\end{gathered}\tag{2.1}$$

where $\boldsymbol{f}_i\left(\boldsymbol{u}\left(\boldsymbol{x}^c,t\right)\right)\in\mathbb{R}^{1\times d}$ stores the fluxes in each of the d directions for the ith state variable, u_i is the ith conserved variable, n_{state} represents the number of state variables, and the superscript c refers to Cartesian coordinates. In this paper, we use row vector notation.

Smooth solutions of Eq. (2.1) satisfy the entropy equality

$$\frac{\partial U}{\partial t}+\nabla\cdot\boldsymbol{F}=0,\ \ \boldsymbol{F}=\boldsymbol{F}(u),\tag{2.2}$$

where U is a convex function of u. Weak solutions satisfy the entropy inequality

$$\frac{\partial U}{\partial t}+\nabla\cdot\boldsymbol{F}\leq 0.\tag{2.3}$$

In the context of entropy-conservative numerical schemes, Mock (1980) and Harten (1983) showed that the symmetrization of the partial differential equation by the entropy variables $\boldsymbol{v}=U'(\boldsymbol{u})$, $\boldsymbol{v}\in\mathbb{R}^{1\times n_{\text{state}}}$, along with the convexity of the entropy function U, leads to the existence of an entropy flux function $\boldsymbol{F}(\boldsymbol{u})$ such that, in each physical direction $k\in[1,d]$,

$$\boldsymbol{v}\frac{\partial \boldsymbol{f}^k{}^T}{\partial \boldsymbol{u}}=\frac{dF^k(\boldsymbol{u})}{d\boldsymbol{u}},\quad \text{where}\left(\frac{\partial \boldsymbol{f}^k{}^T}{\partial \boldsymbol{u}}\right)_{ij}=\frac{\partial f_i^k(\boldsymbol{u})}{\partial u_j},\ \forall i,j\in[1,n_{\text{state}}].\tag{2.4}$$

Harten (1983, Eq. (1.13b)) integrated Eq. (2.4) with respect to the conservative variables and introduced the entropy potential $\boldsymbol{\psi}(\boldsymbol{v})$ such that $(d\psi^k(\boldsymbol{v}))/d\boldsymbol{v}=\boldsymbol{f}^k(\boldsymbol{u}(\boldsymbol{v}))$, arriving at

$$\psi^k(\boldsymbol{v})=\boldsymbol{v}\boldsymbol{f}^k{}^T-F^k(\boldsymbol{u}),\ \forall k\in[1,d].\tag{2.5}$$

Tadmor (1987, Eq. (4.5a)) then demonstrated entropy conservation if

$$\boldsymbol{v}\Delta\left(\boldsymbol{f}^k{}^T\right)=\Delta\left(F^k\right).\tag{2.6}$$

Eq. (2.6) is a strong condition on the flux. Tadmor (1987, Eq. (4.5b)) applied the Δ operator on Eq. (2.5) to obtain the weak condition,

$$\Delta\left(\boldsymbol{v}\right)\boldsymbol{f}^k{}^T=\Delta\left(\psi^k\right).\tag{2.7}$$

Eq. (2.7) is the Tadmor shuffle condition. We introduce $[\![\boldsymbol{v}]\!]=\boldsymbol{v}_i-\boldsymbol{v}_j$ as the jump. The two-point flux $\boldsymbol{f}_s^k(\boldsymbol{v}_i,\boldsymbol{v}_j)$,

$$[\![\boldsymbol{v}]\!]\boldsymbol{f}_s^k(\boldsymbol{v}_i,\boldsymbol{v}_j)^T=[\![\psi^k]\!],\ \forall k\in[1,d],\tag{2.8}$$

is EC (Tadmor 1987; Chan 2018) in discretizations that globally conserve the integrated entropy equality, $\int_{\boldsymbol{\Omega}}(\partial U/\partial t)d\boldsymbol{\Omega}+\int_{\boldsymbol{\Gamma}}\left(\boldsymbol{v}\boldsymbol{f}^T-\boldsymbol{\psi}\right)\cdot\hat{\boldsymbol{n}}\,d\boldsymbol{\Gamma}=0$, exactly in the absence of shocks.

In this research brief, we consider the unsteady Euler equations,

$$\begin{aligned}
\frac{\partial \boldsymbol{W}^T}{\partial t} + \nabla \cdot \boldsymbol{f}\left(\boldsymbol{W}\right)^T &= \boldsymbol{0}^T, \\
\boldsymbol{W} &= \left[\rho, \quad \rho u, \quad \rho v, \quad \rho w, \quad \rho e\right], \\
\boldsymbol{f}_1 &= \left[\rho u, \quad \rho u^2 + p, \quad \rho uv, \quad \rho uw, \quad \left(\rho e + p\right) u\right], \\
\boldsymbol{f}_2 &= \left[\rho v, \quad \rho uv, \quad \rho v^2 + p, \quad \rho vw, \quad \left(\rho e + p\right) v\right], \\
\boldsymbol{f}_3 &= \left[\rho w, \quad \rho uw, \quad \rho vw, \quad \rho w^2 + p, \quad \left(\rho e + p\right) w\right],
\end{aligned} \tag{2.9}$$

where $\rho e = p/(\gamma - 1) + (1/2)\rho\left(u^2 + v^2 + w^2\right)$ and ρ, u, v, w, p, e, and γ are the density, velocity in the x, y, and z directions respectively, pressure, specific total energy, and adiabatic coefficient, respectively.

The kinetic energy is $\mathrm{KE} = (1/2)\rho\left(u^2 + v^2 + w^2\right)$, and the scheme is KEP if

$$\int_{\boldsymbol{\Omega}} \frac{\partial_{\mathrm{KE}}}{\partial t} d\boldsymbol{\Omega} = \int_{\boldsymbol{\Omega}} p \nabla \cdot \mathbf{v} d\boldsymbol{\Omega} - \int_{\boldsymbol{\Gamma}} p \mathbf{v} \cdot \hat{\boldsymbol{n}} d\boldsymbol{\Gamma} \leq 0, \tag{2.10}$$

where the pressure body forces vanish for incompressible flows. The conditions in Eqs. (2.3) and (2.10) provide a bound on the L2 norm of the conserved variables and, thus, provide nonlinear stability—assuming the positivity of density and pressure.

2.1. *Numerical discretization*

The focus of this research brief is on the form of evaluating the two-point flux and the additional constraint provided through the KMP framework. The proposed approach is applicable in finite-volume, finite-difference, and finite-element methods, provided that they are expressed in skew-symmetric form with an SBP property. For completeness, we introduce the skew-symmetric NSFR method that is used to obtain the numerical results.

The computational domain $\boldsymbol{\Omega}^h$ is partitioned into M nonoverlapping elements, $\boldsymbol{\Omega}_m$, where the domain is represented by the union of the elements, $\boldsymbol{\Omega} \simeq \boldsymbol{\Omega}^h \coloneqq \bigcup_{m=1}^{M} \boldsymbol{\Omega}_m$. Each element m has a surface denoted by $\boldsymbol{\Gamma}_m$. The global approximation, $u^h(\boldsymbol{x}^c, t)$, is constructed from the direct sum of each local approximation, $u_m^h(\boldsymbol{x}^c, t)$; that is,

$$u(\boldsymbol{x}^c, t) \simeq u^h(\boldsymbol{x}^c, t) = \bigoplus_{m=1}^{M} u_m^h(\boldsymbol{x}^c, t). \tag{2.11}$$

On each element, we represent the solution with N_p linearly independent modal or nodal basis functions of a maximum order of p, where $N_p \coloneqq (p+1)^d$ for tensor-product elements. The solution representation is $u_m^h(\boldsymbol{x}^c, t) \coloneqq \sum_{i=1}^{N_p} \chi_{m,i}(\boldsymbol{x}^c)\hat{u}_{m,i}(t)$, where $\hat{u}_{m,i}(t)$ are the modal coefficients for the solution. The elementwise residual for the governing equation (Eq. (2.1)) is

$$R_m^h(\boldsymbol{x}^c, t) = \frac{\partial}{\partial t} u_m^h(\boldsymbol{x}^c, t) + \nabla \cdot \boldsymbol{f}(u_m^h(\boldsymbol{x}^c, t)). \tag{2.12}$$

According to Cicchino & Nadarajah (2025), the uncollocated NSFR scheme that discretely solves the residual in Eq. (2.12) is

$$(\boldsymbol{M}_m + \boldsymbol{K}_m)\,\frac{d}{dt}\hat{\boldsymbol{u}}_m(t)^T = -\left[\boldsymbol{\chi}(\boldsymbol{\xi}_v^r)^T\,\boldsymbol{\chi}(\boldsymbol{\xi}_f^r)^T\right]\left[\left(\tilde{\boldsymbol{Q}} - \tilde{\boldsymbol{Q}}^T\right)\odot \boldsymbol{F}_m^r\right]\mathbf{1}^T - \sum_{f=1}^{N_f}\sum_{k=1}^{N_{fp}} \boldsymbol{\chi}(\boldsymbol{\xi}_{fk}^r)^T W_{fk}\hat{\boldsymbol{n}}^r \cdot \boldsymbol{f}_m^{*,r}. \tag{2.13}$$

Here, $\boldsymbol{M}_m + \boldsymbol{K}_m$ is the flux reconstruction modified mass matrix (Allaneau & Jameson 2011; Cicchino *et al.* 2022a,b; Cicchino & Nadarajah 2025), and $\tilde{\boldsymbol{Q}} - \tilde{\boldsymbol{Q}}^T$ is the general hybridized skew-symmetric stiffness operator involving both volume and surface quadrature evaluations (Chan 2019) wherein each $\tilde{\boldsymbol{Q}}$ satisfies the SBP property. $\boldsymbol{\chi}(\boldsymbol{\xi}_v^r)$ and $\boldsymbol{\chi}(\boldsymbol{\xi}_f^r)$ are the basis functions evaluated at the volume and surface quadrature nodes, respectively. For the discrete surface integral, W_{fk} are the quadrature weights and $\boldsymbol{f}_m^{*,r}$ is the surface numerical flux transformed to the reference space.

The discretization in Eq. (2.13) has been proven and numerically validated to discretely conserve entropy, kinetic energy, global conservation, and freestream preservation (Cicchino & Nadarajah 2025). It has also had its orders of convergence extensively verified (Cicchino *et al.* 2022a,b; Cicchino & Nadarajah 2025), and the operations scale at $\mathcal{O}\left(n^{d+1}\right)$ through sum-factorization algorithms for both matrix-vector multiplications and the Hadamard product (Cicchino & Nadarajah 2024, 2025).

3. Kovasznay mode preservation

Kovasznay (1953) linearly decomposed isotropic turbulence into acoustic, vortical, and entropic modes. Ribner (1954) then derived LIA by modeling the interaction between isotropic turbulence and a shock wave as the interaction of each linear Kovasznay mode and the shock wave independently. Note that each mode produces all three modes downstream of the shock from the interaction process. LIA has been extensively verified with respect to direct numerical simulations (Lee *et al.* 1993, 1997; Mahesh *et al.* 1995, 1997; Larsson & Lele 2009; Bermejo & Lele 2010) and has proven to be a reliable model for predicting postshock kinetic energy amplification (Cuadra *et al.* 2025).

For the compressible Euler equations, we assume that the flow solution can be decomposed into a mean base state and a perturbation, $\rho = \bar{\rho} + \rho'$, $u = \bar{u} + u'$, $p = \bar{p} + p'$, and $s = \bar{s} + s'$. By substituting the linearized modes into Eq. (2.9), we arrive at three linearly independent equations for the advection of the perturbations (Kovasznay 1953),

$$\begin{aligned} \frac{\partial \rho'}{\partial t} + \bar{u}\frac{\partial \rho'}{\partial x} &= -\bar{\rho}\frac{\partial u'}{\partial x}, \\ \bar{\rho}\left(\frac{\partial u'}{\partial t} + \bar{u}\frac{\partial u'}{\partial x}\right) &= -\frac{\partial p'}{\partial x}, \\ \frac{\partial s'}{\partial t} + \bar{u}\frac{\partial s'}{\partial x} &= 0. \end{aligned} \tag{3.1}$$

For the numerical discretization, in the small-perturbation limit, we conjecture that the aliasing errors associated with each mode should obey Eq. (3.1). To have the discretization accomplish this goal, we derived the following weak conditions for the discrete flux.

3.1. *Acoustic mode*

The acoustic mode is assumed to be inviscid, isentropic, and adiabatic, thus satisfying the barotropic condition, $p = \kappa\rho^\gamma$ (where κ is a constant). It has no perturbations in

vorticity or entropy; that is, $\omega' = 0$ and $s' = 0$. Discretely, zero perturbations for the vorticity and entropy is preserved by discretely conserving the material derivative, with $D/Dt = \partial/\partial t + \mathbf{v} \cdot \nabla$, of the entropy and vorticity for only the acoustic mode. The acoustic mode conditions, therefore, are

$$\int_{\mathbf{\Omega}} \frac{Ds}{Dt} d\mathbf{\Omega} = 0, \quad \int_{\mathbf{\Omega}} \frac{D\boldsymbol{\omega}}{dt} d\mathbf{\Omega} = \int_{\mathbf{\Omega}} (\omega \cdot \nabla)\, \mathbf{v} - \omega\, (\nabla \cdot \mathbf{v}) + \frac{1}{\rho^2} \nabla\rho \times \nabla p d\mathbf{\Omega} = \mathbf{0}. \tag{3.2}$$

Discretely, the numerical scheme preserves the acoustic mode if, after substituting a barotropic flow assumption, all of the discrete terms vanish in Eq. (3.2). Eq. (3.2) provides L2 bounds on the time rate of change of the entropy and vorticity associated with an acoustic mode; that is, $d/dt\|\rho s\|_2^2 \leq 0$, and $d/dt\|\boldsymbol{\omega}\|_2^2 \leq \mathbf{0}$. Gassner *et al.* (2016) numerically demonstrated that using the average of the pressure terms in the convective flux leads to a more accurate long-time conservation of kinetic energy for the inviscid Taylor–Green vortex. For the inviscid Taylor–Green vortex problem, kinetic energy should be conserved to machine precision because there are no viscous terms and the density analytically remains constant. Numerically, it does not stay at machine precision when solved by a compressible flow solver because the solver does not enforce incompressibility and, thus, the numerical source term from the pressure in Eq. (2.10) is not exactly zero. On the basis of these results, Ranocha (2018)and Ranocha & Gassner (2022) incorporated the average of the pressure in the kinetic energy preservation condition. According to Eq. (2.10), no condition is needed for the pressure to conserve kinetic energy (Jameson 2008). Numerically, use of the arithmetic averages for the pressure is preferable for advecting acoustic modes,and was an important component in the derivation of the convective-upwind-split-pressure scheme (Jameson 1993, 1995a,b). Eq (3.2) shows that using the average of the pressure prevents an artificial baroclinic force, $(1/\rho^2)\nabla\rho \times \nabla p$, from being introduced by the numerical discretization when advecting an acoustic mode.

Theorem 3.1. Using the arithmetic average for the discrete pressure in the two-point flux for the momentum equations prevents an artificial baroclinic force from being introduced by the propagation of aliasing errors associated with an acoustic mode.

Proof. We start with the non-chain-rule form of the baroclinic force,

$$-\frac{1}{\rho^2}\nabla\rho \times \nabla p = \nabla \times \left(\frac{1}{\rho}\nabla p\right), \tag{3.3}$$

which we expand discretely in two dimensions with the arithmetic average for the pressure,

$$\left(\nabla \times \left(\frac{1}{\rho}\nabla p\right)\right)_k = \sum_i D^x_{ki} \frac{1}{\rho_i} \sum_j 2D^y_{ij} \frac{1}{2} (p_i + p_j) - \sum_i D^y_{ki} \frac{1}{\rho_i} \sum_j 2D^x_{ij} \frac{1}{2} (p_i + p_j), \tag{3.4}$$

where $D^x_{ij} = (\partial\chi_i(\boldsymbol{\xi}^r_j))/\partial x$ is the derivative of the ith basis function at the jth node in the x direction, and similarly for D^y_{ij}. Using the fact that $\sum_j D_{ij} = 0$, we simplify to

$$\left(\nabla \times \left(\frac{1}{\rho}\nabla p\right)\right)_k = \sum_i D^x_{ki} \frac{1}{\rho_i} \sum_j D^y_{ij} (p_j) - \sum_i D^y_{ki} \frac{1}{\rho_i} \sum_j D^x_{ij} (p_j). \tag{3.5}$$

We then substitute the fact that the flow is barotropic, $p = \kappa\rho^\gamma$, by assuming an inviscid, isentropic, and adiabatic flow, and integrate with respect to ρ^γ,

$$\int_{\mathbf{\Omega}} \rho^\gamma \nabla \times \left(\frac{1}{\rho}\nabla p\right) d\mathbf{\Omega} = \sum_k \sum_i \sum_j \rho_k^\gamma W_k \left[D_{ki}^x \frac{1}{\rho_i} D_{ij}^y \left(\kappa\rho_j^\gamma\right) - D_{ki}^y \frac{1}{\rho_i} D_{ij}^x \left(\kappa\rho_j^\gamma\right)\right]. \quad (3.6)$$

We integrate with respect to ρ^γ because it is positive and real valued for compressible flows everywhere and the preservation of the vorticity equation is proven in the ρ^γ-weighted L2 norm. Lastly, we perform discrete integration by parts on both terms, provided that the quadrature rule is exact for polynomials of order $2p-1$. The remaining volume terms are

$$\sum_k \sum_i \sum_j -\rho_k^\gamma D_{ik}^x W_i \frac{1}{\rho_i} D_{ij}^y \left(\kappa\rho_j^\gamma\right) + \rho_k^\gamma D_{ik}^y W_i \frac{1}{\rho_i} D_{ij}^x \left(\kappa\rho_j^\gamma\right) = 0, \quad (3.7)$$

and the volume terms discretely cancel because they are the transpose of one another. The remaining surface terms cancel with the surface numerical flux after summing over all elements. The same result holds for three dimensions. Thus, the arithmetic average for the pressure flux in the momentum equations provably does not introduce a fictitious baroclinic force for the transport of an acoustic mode.

□

Theorem (3.1) provides the additional constraint on the pressure discretization for the EC, KEP, and KMP flux. Additionally, Theorem (3.1) is needed to prove conservation of the acoustic mode conditions.

3.2. *Vortical mode*

The vortical mode is defined by an isentropic, inviscid, and adiabatic flow with no pressure or entropic perturbations, $p' = 0$ and $s' = 0$. The conservation laws that preserve these perturbation properties are the material derivative of the entropy and potential vorticity, $q = (\boldsymbol{\omega} \cdot \nabla s)/\rho$. The potential vorticity measures the amount of spin a fluid parcel has with respect to its compression and stratification. It also drives the generation of vorticity by baroclinic torques when present, propagates Rossby waves, and develops cyclogenesis. The vortical mode conditions are

$$\int_{\mathbf{\Omega}} \frac{Dq}{Dt} d\mathbf{\Omega} = 0, \quad \int_{\mathbf{\Omega}} \frac{Ds}{Dt} d\mathbf{\Omega} = 0. \quad (3.8)$$

Equation (3.8) provides L2 bounds on the time rate of change of the entropy and potential vorticity associated with a vortical mode, namely $d/dt\|\rho s\|_2^2 \leq 0$ and $d/dt\|\rho q\|_2^2 \leq 0$.

3.3. *Entropic mode*

Lastly, the entropic mode is defined by having no vortical or pressure perturbations, $\omega' = 0$ and $p' = 0$, which results in the pressure equilibrium conditions (Shima *et al.* 2021; Ranocha & Gassner 2022). The entropic mode conditions are

$$\int_{\mathbf{\Omega}} \frac{\partial p}{\partial t} d\mathbf{\Omega} = 0, \quad \int_{\mathbf{\Omega}} \frac{\partial \mathbf{v}}{\partial t} d\mathbf{\Omega} = \mathbf{0}. \quad (3.9)$$

Equation (3.9) provides L2 bounds on the time rate of change of the pressure and

velocity associated with an entropic mode, namely $d/dt\|p\|_2^2 \leq 0$ and $d/dt\|\boldsymbol{v}\|_2^2 \leq \mathbf{0}$. Together, Eqs. (3.2) and (3.8-3.9) are the KMP conditions. One can show that the EC and KEP flux of Ranocha & Gassner (2022) is KMP. For the advection of the density wave from Gassner *et al.* (2022), KMP provides an alternative interpretation as to why the method crashes with the flux of Ranocha & Gassner (2022). For the test from Gassner *et al.* (2022), the density variation in the flow is itself an entropic wave, and its advection is preserved by numerical methods that preserve the entropic mode conditions in Eq. (3.9), such as the flux of Ranocha & Gassner (2022) and Shima *et al.* (2021). Use of the KMP flux for the specific configuration of the density, pressure, and velocity in the test case of Gassner *et al.* (2022) still crashes because it is the advection of an extremely sharp temperature gradient with a two-order-of-magnitude jump in the difference. KMP, entropy stability, and kinetic energy stability do not prevent spurious modes from appearing at sharp gradients and discontinuities.

4. Results

All numerical results were obtained using `PHiLiP` (Shi-Dong & Nadarajah 2021; Cicchino 2024) with Gauss–Lobatto–Legendre quadrature nodes, Lagrange polynomial basis functions, c_{DG} for the flux reconstruction parameter, and the positivity-preserving limiter (Zhang & Shu 2010, 2011a,b; Srinivasan & Nadarajah 2025). The surface numerical flux uses Roe (1981) upwinding with the chosen baseline two-point flux that is EC, KMP, and/or KEP. All tests use a time step that is adapted by the maximum wave speed in the domain and the strong stability–preserving third-order Runge–Kutta method (Gottlieb & Shu 1998; Gottlieb *et al.* 2011).

We investigate the impact of KMP downstream of an unsteady shock interaction by considering the interaction with an entropy wave and a vortical perturbation. This is important because, in an LES of shock–turbulence interaction, the flow will be underresolved and the aliasing errors must be propagated in a way that does not negatively affect the subgrid-scale closures.

First, we consider the Shu–Osher test, where a one-dimensional entropy wave interacts with a shock and produces both entropic and acoustic waves postshock. The initial conditions are

$$(\rho, u, p) = \begin{cases} (3.857143, 2.629369, 10.33333)), \text{ if } x < -4, \\ (1 + 0.2\sin 5x, 0, 1) \text{ if } x \geq 4. \end{cases} \tag{4.1}$$

In Figure 1, we compare a few popular choices of two point fluxes at time $t_f = 1.8$ s to highlight the effect of KMP. In black, we plot the different solutions obtained by different fluxes, and in red, we plot a reference solution using DG, with no shock capturing, so it still has a few oscillations at the interface between the contact discontinuity and acoustic wave ($p = 1$ and 2500) elements. We use a Courant-Friedrichs-Lewy (CFL) of 0.2. There's the kinetic energy preservning (KEP), approximately entropy-stable flux, KEP, approx. EC, not KMP (Jain & Moin 2022; Shima *et al.* 2021); the flux of Chandrashekar (2013), EC, KEP, not KMP, which is not KMP because it does not preserve the acoustic mode and introduces additional fictitious baroclinic forces; and the EC, KEP, KMP flux of Ranocha & Gassner (2022). These are compared with a baseline DG scheme for the same polynomial order and grid size that does not have a stability bound. All were run with 100 elements of equal size.

According to Figure 1(a)-(d) all methods show small spurious modes at the shock–

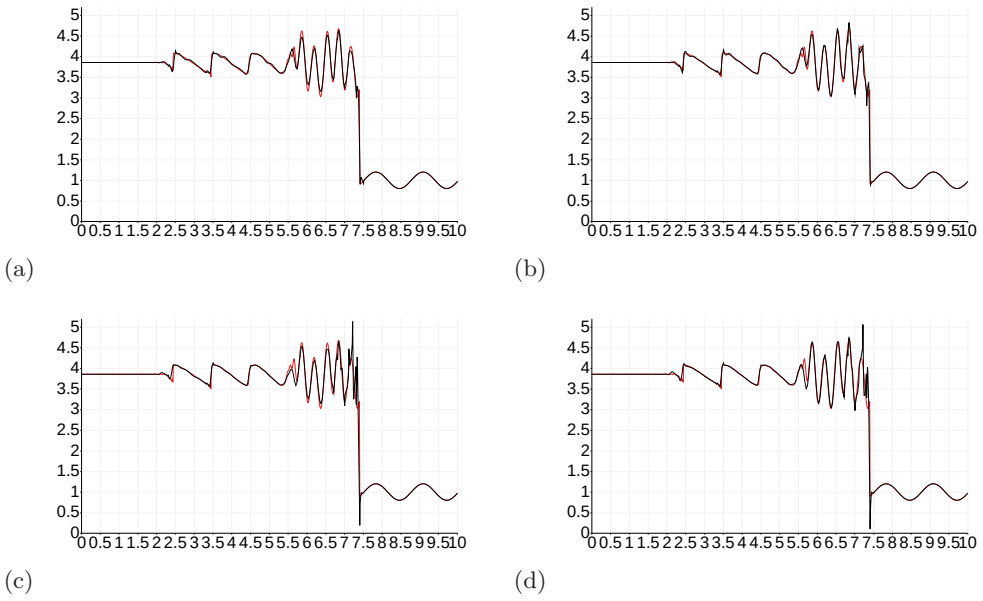

Figure 1: Density plots for the Shu-Osher test. (a) Baseline DG, (b) KEP, approximately EC, not KMP, (c) EC, KEP, not KMP, (d) and EC, KEP, KMP. This figure compares four choices of two-point fluxes with a reference solution.

entropic mode interface and at the heads and tails of the contact discontinuities. None of the schemes have any shock-capturing mechanism in place that would suppress the growth of spurious modes. This choice was made in accordance with Section 3 because Section 3 predicted that the fluxes that violate the KMP conditions would introduce fictitious forces associated with each Kovasznay mode the discretization violates. The KMP flux closely captures the contact discontinuities and the acoustic wave up until the shock. For higher polynomial orders, more oscillations are present for all methods, and all methods are oscillatory in pressure at the location of the interface between the shock and the acoustic wave. Also, for physically relevant flows, shock capturing in the form of a limiter, filter, artificial viscosity, or adaptive stencil would be needed to control the growth of spurious oscillations.

Next, we consider the two-dimensional shock–vortex interaction. The domain is $[0, 2] \times [0, 1]$, 50 elements are used in the x direction, 25 elements are used in the y direction, and $p = 4$. The grid-converged reference solution is that of Srinivasan & Nadarajah (2025), who use 100×250 elements and $p = 3$. We compare this solution with the three choices of fluxes using an underresolved $p = 4$ and 50×25 elements.

The test case involves a stationary shock $M_s = 1.5$ at $x = 0.5$ and a strong vortex $M_v = 0.9$ centered at $(0.25, 0.5)$. The inlet is supersonic, the outlet is subsonic, and the top and bottom are wall boundary conditions. The vortex passes through the shock wave, the shock corrugates, and the interaction produces all three modes—vortical, entropic, and acoustic—downstream of the shock. All three modes interact with one another nonlinearly. Figure 2(a)-(d) plots the density contours at $t_f = 0.7$ s using CFL $= 0.5$.

Because no shock capturing is present, all schemes produce spurious modes during the interaction with the shock. From the KMP analysis, the KEP, approx. EC, not KMPflux does not preserve the material derivative of the entropy. Thus, the linearly

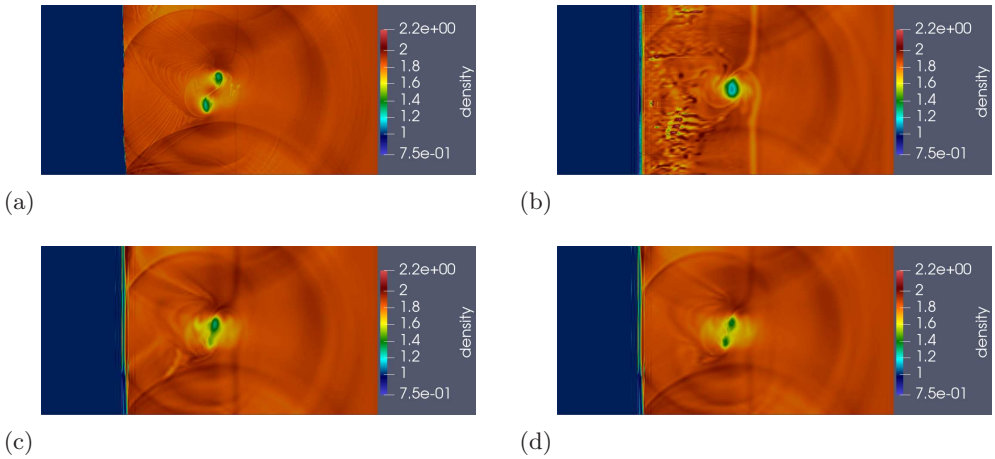

Figure 2: Density contours for the shock-vortex interaction at $t = 0.7$ s. (a) Grid-converged, fully resolved reference solution from Figure 13 Srinivasan & Nadarajah (2025), (b) KEP, approximately EC, not KMP, (c) KEP, EC, not KMP, (d) and KEP, EC, KMP. This figure compares the under-resolved solutions with three different two-point flux choices with a grid-converged, fully resolved reference solution.

perturbed system from the interaction with the shock propagates the spurious modes downstream in the form of additional entropy waves. The spurious modes in Figure 2(b) resemble entropy waves. Although there is a physical baroclinic torque present in the flow because the problem is not isentropic; the EC, KEP, not KMP flux does not preserve the acoustic wave and provably creates an additional fictitious baroclinic torque from the spurious modes downstream of the shock, in accordance with Theorem 3.1. This additional torque is observed to the left of the vortex in Figure 2(c) and prevents it from splitting. In comparison, the EC, KEP, KMP flux is the closest to resembling the downstream advection of a filtered field of the grid-converged result. For LES, results are commonly compared with a direct numerical simulation filtered to the same number of degrees of freedom. Here, we compare the L2 errors between the final solutions from the underresolved simulation with a Gaussian-filtered field of the grid-converged solution: KEP, approx. EC, not KMP, 6.95e-2; EC, KEP, not KMP, 3.53 e-2; and EC, KEP, KMP, 2.95 e-2. The L2 errors were computed for all values to the right of the shock by applying a Gaussian filter with filter width 3.58 that corresponds to the difference in degrees of freedom, and then interpolating the filtered field to the coarse mesh. The KMP flux results are the closest to the filtered grid-converged solution, demonstrating that the physical forces present in the underresolved simulation most closely resemble a filtered approximation of the grid-converged solution.

5. Conclusions

This paper introduced KMP as an additional set of physical constraints to be used in combination with entropy stability and kinetic energy preservation. KMP was derived so that the aliasing errors present in the discretization propagate according to Kovasnzay's modal decomposition. This process resulted in three sets of additional conservation laws that the numerical scheme must discretely satisfy for the acoustic, vortical, and entropic

modes independently. Additionally, from the acoustic mode condition, we proved in Theorem (3.1) that the arithmetic average for the pressure in the momentum equations does not generate an additional fictitious baroclinic torque in the flow. The numerical results verify that the KMP framework accurately predicted the presence and the types of additional fictitious forces in the numerical approximation caused by dispersive errors. Tests on physically relevant flows are needed to validate KMP and measure its impact. The future outlook of the method is that KMP provides a framework that decouples the numerical aliasing errors from the subgrid closures for linearly perturbed flows, which should be used together with a form of shock capturing for physically relevant flows. The outstanding major question concerns the impact on statistical quantities of interest, like postshock kinetic energy amplification, and the role of incorporating LIA into subgrid-scale models for LES of shock–turbulence problems.

Acknowledgments

The support of the US Office of Naval Research to the Center for Turbulence Research (grant N000142312833) is gratefully acknowledged. The first author thanks Chris Williams for fruitful discussions on linear interaction analysis and shock–turbulence interaction. The first author also thanks Sai Shruthi Srinivasan.

REFERENCES

Abgrall, R. 2018 A general framework to construct schemes satisfying additional conservation relations. Application to entropy conservative and entropy dissipative schemes. *J. Comput. Phys.* **372**, 640–666.

Abgrall, R., Nordström, J., Öffner, P. & Tokareva, S. 2021 Analysis of the SBP-SAT stabilization for finite element methods. Part II: Entropy stability. *Commun. Appl. Math. Comput.* **5**, 573–595.

Abgrall, R., Öffner, P. & Ranocha, H. 2022 Reinterpretation and extension of entropy correction terms for residual distribution and discontinuous Galerkin schemes: application to structure preserving discretization. *J. Comput. Phys.* **453**, 110955.

Allaneau, Y. & Jameson, A. 2011 Connections between the filtered discontinuous Galerkin method and the flux reconstruction approach to high order discretizations. *Comput. Methods Appl. Mech. Eng.* **200**, 3628–3636.

Bermejo, I. & Lele, S. 2010 LES of canonical shock-turbulence interaction. *Annual Research Briefs,* Center for Turbulence Research, Stanford University, p. 209 - 222.

Chan, J. 2018 On discretely entropy conservative and entropy stable discontinuous Galerkin methods. *J. Comput. Phys.* **362**, 346–374.

Chan, J. 2019 Skew-symmetric entropy stable modal discontinuous Galerkin formulations. *J. Sci. Comput.* **81**, 459–485.

Chandrashekar, P. 2013 Kinetic energy preserving and entropy stable finite volume schemes for compressible Euler and Navier–Stokes equations. *Comm. Comput. Phys.* **14**, 1252–1286.

Cicchino, A. 2024 Weight-adjusted nonlinearly stable flux reconstruction high-order methods for compressible flows in curvilinear coordinates. PhD Dissertation, McGill University.

Cicchino, A., Del Rey Fernández, D. C., Nadarajah, S., Chan, J. & Carpenter, M. H. 2022a Provably stable flux reconstruction high-order methods on curvilinear elements. *J. Comput. Phys.* **463**, 111259.

Cicchino, A. & Nadarajah, S. 2024 Scalable evaluation of hadamard products with tensor product basis for entropy-stable high-order methods. *J. Comput. Phys.* **513**, 113134.

Cicchino, A. & Nadarajah, S. 2025 Discretely nonlinearly stable weight-adjusted flux reconstruction high-order method for compressible flows on curvilinear grids. *J. Comput. Phys.* **521**, 113532.

Cicchino, A., Nadarajah, S. & Del Rey Fernández, D. C. 2022b Nonlinearly stable flux reconstruction high-order methods in split form. *J. Comput. Phys.* **458**, 111094.

Cuadra, A., Di Renzo, M., Hoste, J.-J. O., Williams, C. T., Vera, M. & Huete, C. 2025 Review of shock-turbulence interaction with a focus on hypersonic flow. *Phys. Fluids* **37**, 045129.

Fisher, T. C. & Carpenter, M. H. 2013 High-order entropy stable finite difference schemes for nonlinear conservation laws: finite domains. *J. Comput. Phys.* **252**, 518–557.

Gassner, G. J. 2013 A skew-symmetric discontinuous Galerkin spectral element discretization and its relation to SBP-SAT finite difference methods. *SIAM J. Sci. Comput.* **35**, A1233–1253.

Gassner, G. J., Svärd, M. & Hindenlang, F. J. 2022 Stability issues of entropy-stable and/or split-form high-order schemes. *J. Sci. Comput.* **90**, 1–36.

Gassner, G. J., Winters, A. R. & Kopriva, D. A. 2016 Split form nodal discontinuous Galerkin schemes with summation-by-parts property for the compressible Euler equations. *J. Comput. Phys.* **327**, 39–66.

Goc, K. A., Lehmkuhl, O., Park, G. I., Bose, S. T. & Moin, P. 2021 Large eddy simulation of aircraft at affordable cost: a milestone in computational fluid dynamics. *Flow* **1**, E14.

Gottlieb, S., Ketcheson, D. I. & Shu, C.-W. 2011 *Strong Stability Preserving Runge–Kutta and Multistep Time Discretizations*. World Scientific.

Gottlieb, S. & Shu, C.-W. 1998 Total variation diminishing Runge-Kutta schemes. *Math. Comput.* **67**, 73–85.

Ham, F., Mattsson, K., Iaccarino, G. & Moin, P. 2007 Towards time-stable and accurate LES on unstructured grids. In *Complex Effects in Large Eddy Simulations*, ed. S. C. Kassinos, C. A. Langer, G. Iaccarino & P. Moin, pp. 235–249. Springer.

Harten, A. 1983 On the symmetric form of systems of conservation laws with entropy. *J. Comput. Phys.* **49**, 151–164.

Honein, A. E. & Moin, P. 2004 Higher entropy conservation and numerical stability of compressible turbulence simulations. *J. Comput. Phys.* **201**, 531–545.

Jain, S. S. & Moin, P. 2022 A kinetic energy– and entropy-preserving scheme for compressible two-phase flows. *J. Comput. Phys.* **464**, 111307.

Jameson, A. 1993 Artificial diffusion, upwind biasing, limiters and their effect on accuracy and multigrid convergence in transonic and hypersonic flows. *AIAA Paper 93-3359*.

Jameson, A. 1995a Analysis and design of numerical schemes for gas dynamics. 1. Artificial diffusion, upwind biasing, limiters and their effect on accuracy and multigrid convergence. *Int. J. Comput. Fluid Dyn.* **4**, 171–218.

Jameson, A. 1995b Analysis and design of numerical schemes for gas dynamics. 2. Artificial diffusion and discrete shock structure. *Int. J. Comput. Fluid Dyn.* **5**, 1–38.

Jameson, A. 2008 Formulation of kinetic energy preserving conservative schemes for gas dynamics and direct numerical simulation of one-dimensional viscous compressible flow in a shock tube using entropy and kinetic energy preserving schemes. *J. Sci. Comput.* **34**, 188–208.

Johnsen, E., Larsson, J., Bhagatwala, A. V., Cabot, W. H., Moin, P., Olson, B. J., Rawat, P. S., Shankar, S. K., Sjögreen, B., Yee, H. C., Zhong, X. & Lele, S.K. 2010 Assessment of high-resolution methods for numerical simulations of compressible turbulence with shock waves. *J. Comput. Phys.* **229**, 1213–1237.

Kovasznay, L. S. 1953 Turbulence in supersonic flow. *J. Aeronaut. Sci.* **20**, 657–674.

Larsson, J. & Lele, S. K. 2009 Direct numerical simulation of canonical shock/turbulence interaction. *Phys. Fluids* **21**, 126101.

Lee, S., Lele, S. K. & Moin, P. 1993 Direct numerical simulation of isotropic turbulence interacting with a weak shock wave. *J. Fluid Mech.* **251**, 533–562.

Lee, S., Lele, S. K. & Moin, P. 1997 Interaction of isotropic turbulence with shock waves: effect of shock strength. *J. Fluid Mech.* **340**, 225–247.

LeFloch, P. G., Mercier, J.-M. & Rohde, C. 2002 Fully discrete, entropy conservative schemes of arbitrary order. *SIAM J. Numer. Anal.* **40**, 1968–1992.

LeFloch, P. G. & Rohde, C. 2000 High-order schemes, entropy inequalities, and nonclassical shocks. *SIAM J. Numer. Anal.* **37**, 2023–2060.

Mahesh, K., Constantinescu, G., Apte, S., Iaccarino, G., Ham, F. & Moin, P. 2006 Large-eddy simulation of reacting turbulent flows in complex geometries. *J. Appl. Mech.* **73**, 374–381.

Mahesh, K., Lee, S., Lele, S. K. & Moin, P. 1995 The interaction of an isotropic field of acoustic waves with a shock wave. *J. Fluid Mech.* **300**, 383–407.

Mahesh, K., Lele, S. K. & Moin, P. 1997 The influence of entropy fluctuations on the interaction of turbulence with a shock wave. *J. Fluid Mech.* **334**, 353–379.

Mock, M. S. 1980 Systems of conservation laws of mixed type. *J. Differ. Equ.* **37**, 70–88.

Moin, P. 2002 Advances in large eddy simulation methodology for complex flows. *Int. J. Heat Fluid Flow* **23**, 710–720.

Moin, P. & Apte, S. V. 2006 Large-eddy simulation of realistic gas turbine combustors. *AIAA J.* **44**, 698–708.

Montoya, T. & Zingg, D. W. 2024 Efficient tensor-product spectral-element operators with the summation-by-parts property on curved triangles and tetrahedra. *SIAM J. Sci. Comput.* **46**, A2270–2297.

Morinishi, Y., Lund, T. S., Vasilyev, O. V. & Moin, P. 1998 Fully conservative higher order finite difference schemes for incompressible flow. *J. Comput. Phys.* **143**, 90–124.

Nordström, J. 2022 Nonlinear and linearised primal and dual initial boundary value problems: When are they bounded? How are they connected? *J. Comput. Phys.* **455**, 111001.

Ranocha, H. 2018 Comparison of some entropy conservative numerical fluxes for the Euler equations. *J. Sci. Comput.* **76**, 216–242.

Ranocha, H. & Gassner, G. J. 2022 Preventing pressure oscillations does not fix local linear stability issues of entropy-based split-form high-order schemes. *Commun. Appl. Math. Comput.* **4**, 880–903.

Ribner, H. S. 1954 Convection of a pattern of vorticity through a shock wave. Tech. Rep., NASA.

Roe, P. L. 1981 Approximate Riemann solvers, parameter vectors, and difference schemes. *J. Comput. Phys.* **43**, 357–372.

Shi-Dong, D. & Nadarajah, S. 2021 Full-space approach to aerodynamic shape optimization. *Comput. Fluids* **218**, 104843.

Shima, N., Kuya, Y., Tamaki, Y. & Kawai, S. 2021 Preventing spurious pressure oscillations in split convective form discretization for compressible flows. *J. Comput. Phys.* **427**, 110060.

Srinivasan, S. S. & Nadarajah, S. 2025 Investigation of shock-capturing with bound-preserving limiters for the nonlinearly stable flux reconstruction method. arXiv:2507.09131 [math.NA].

Tadmor, E. 1984 Skew-self adjoint form for systems of conservation laws. *J. Math. Anal. Appl.* **103**, 428–442.

Tadmor, E. 1987 The numerical viscosity of entropy stable schemes for systems of conservation laws. I. *Math. Comput.* **49**, 91–103.

Van Ingen, J. 2008 The eN method for transition prediction. Historical review of work at TU Delft. *AIAA Paper 2008-3830*.

Zhang, X. & Shu, C.-W. 2010 On positivity-preserving high order discontinuous Galerkin schemes for compressible Euler equations on rectangular meshes. *J. Comput. Phys.* **229**, 8918–8934.

Zhang, X. & Shu, C.-W. 2011a Maximum-principle-satisfying and positivity-preserving high-order schemes for conservation laws: survey and new developments. *Proc. R. Soc. Lond. A* **467**, 2752–2776.

Zhang, X. & Shu, C.-W. 2011b Positivity-preserving high order discontinuous Galerkin schemes for compressible Euler equations with source terms. *J. Comput. Phys.* **230**, 1238–1248.